ACS APPLIED MATERIALS & INTERFACES

www.acsami.org

Research Article

Polydopamine-Coated Radiolabeled Microspheres for Combinatorial Radioembolization and Photothermal Cancer Therapy

Manran Wu,[#] Lei Zhang,[#] Kexin Shi,[#] Dongxu Zhao, Weipeng Yong, Lingling Yin, Ruizhe Huang, Guanglin Wang,* Gang Huang, and Mingyuan Gao*

Cite This: https://doi.org/10.1021/acsami.2c19829

Read Online

ACCESS | Metrics & More | Article Recommendations | Supporting Information

ABSTRACT: Transarterial radioembolization (TARE) is a local radionuclide therapy and is successfully used in hepatocellular carcinoma (HCC) treatment. Radioactive microspheres have been widely studied for TARE. Preparation of ideal radioactive microspheres is significant for clinical research and patient treatment. In this study, we have designed a novel multifunctional microsphere, i.e., polydopamine (PDA)-coated ^{177}Lu-radiolabeled silica microspheres (MS) denoted as ^{177}Lu-MS@PDA, which can be used for TARE and photothermal therapy (PTT). The radiostability of ^{177}Lu-MS@PDA was significantly improved by coating ^{177}Lu-MS with PDA. In addition, the coating of PDA makes microspheres have excellent photothermal performance. MicroSPECT/CT images showed that ^{177}Lu-MS@PDA was accurately embolized and remained in the tumor during the observation time. At the time, it also showed that ^{177}Lu-MS@PDA was very stable in vivo. Furthermore, the anti-tumor results demonstrated that TARE combined with PTT of ^{177}Lu-MS@PDA can significantly inhibit tumor growth without obvious side effects. ^{177}Lu-MS@PDA holds great potential as a promising radioactive microsphere for HCC.

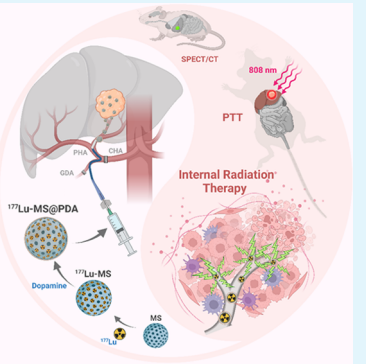

KEYWORDS: *hepatocellular carcinoma, transarterial radioembolization, photothermal therapy, radioactive microspheres, ^{177}Lu radiolabeling*

INTRODUCTION

Hepatocellular carcinoma (HCC) is the most common primary liver malignancy, which causes serious harm to human health.[1,2] However, only about 40% of patients are suitable for surgical resection when they are diagnosed with HCC. Moreover, the 5-year recurrence rate of the patients receiving surgical resection remains as high as 70%.[3−6] Transarterial chemoembolization and transarterial radioembolization (TARE) have been demonstrated to be effective for improving the survival of patients with unresectable HCC.[7−9] TARE maximizes the radiation dose in the tumorous region by selectively injecting radioactive materials, such as microspheres, into the hepatic artery.[10−12]

The commercially available radioactive microspheres mainly chosen are ^{90}Y-labeled glass microspheres (TheraSphere), ^{90}Y-labeled resin microspheres (SIR-Spheres), and ^{166}Ho-labeled poly-L-lactic acid microspheres (QuiremSpheres).[13−15] Among these radioactive microspheres, ^{90}Y-based TheraSphere and SIR-Spheres as pure beta emitters are not suitable for nuclear imaging due to their extremely low positron yield and the absence of gamma rays, which are unfavorable for subsequently monitoring the localization and estimating the local dosimetry. The radioactive microspheres can generally be obtained through direct adsorption of radioisotopes or converting the nonradioactive isotope embedded in the microsphere by neutron activation. The radiostability of the microspheres obtained through the former approach needs to be further improved,[16,17] while the neutron activation may damage the microsphere matrix and produce unwanted long half-life radioisotopes.[15,18,19]

^{90}Y has largely been used in radioactive microspheres so far. However, ^{177}Lu is being considered as an attractive alternative due to its favorable physicochemical properties and good commercial availability. ^{177}Lu emits beta particles (498 keV) and low-energy gamma photons (210 keV (11%), 113 keV (6%)), which can be used for therapy and imaging, respectively.[20,21] Thus, ^{177}Lu becomes a suitable choice for TARE application; however, it requires a reliable radiolabeling technique to avoid unnecessary side effects of the leached radioisotopes to normal tissues.[22,23] To date, there have been a

Received: November 3, 2022
Accepted: February 17, 2023

few studies reported on radioactive microspheres, which remained to be improved with respect to radiostability.[24−26]

In recent years, photothermal therapy (PTT) has been proposed to combine with radiotherapy for improving the therapeutic effects for cancer treatment.[27,28] As a minimally invasive treatment, PTT relies on the conversion of NIR light to heat to effectively kill tumor cells without causing damage to normal tissues.[29,30] Recent studies have shown that a great variety of inorganic nanomaterials can potentially be used as PTT reagents. However, they accumulate in tumors mostly through enhanced permeability and retention effect. Clinical translation is affected by the limited evaluation of bioavailability due to the potential side effects of the nanoagents.[31−33] This disadvantage of current PTT methods may be overcome if PTT agents are combined with radioactive isotopes in a single microsphere as a dual-functional microsphere can be delivered to the tumorous sites through intra-artery administration to avoid non-targeting distribution of the PTT agent. Moreover, it is reasonably expected that the combination of PTT and TARE can further reduce the radiation dose in the treatment and minimize radiation damage to normal tissues.[34] Most importantly, repetitive PTT can facilely enable to suppress the recurrence and eliminate the tumor residual of HCC after radiotherapy.[28]

In this context, it is practically meaningful to combine PTT with TARE by integrating a suitable PTT agent into radioactive microspheres. Polydopamine (PDA) in this respect is an excellent choice due to its remarkable biocompatibility and photothermal conversion capacity.[35−38] Moreover, PDA can not only form an adhesive film on a great variety of solid surfaces but also coordinate firmly with transition and rare earth metal ions, which allows a reasonable hypothesis that can be used to coat the radioactive microspheres, on the one hand to endow the latter with PTT function and on the other hand to suppress leakage of radionuclides for achieving improved therapeutic effects.[39−42] To verify these hypotheses, we herein reported ^{177}Lu-radiolabeled silica microspheres coated with PDA, denoted as ^{177}Lu-MS@PDA, for TARE/PTT of HCC as schematically described in Scheme 1. Silica microspheres have many excellent properties, such as good biocompatibility, large specific surface area, and good ion absorption capacity, and they are good drug carriers.[43] The radiolabeling stability and photothermal performance of the dual-functional microsphere were evaluated in vitro. Rats with N1S1 orthotopic liver cancer were constructed for showing the tumor growth inhibition effects of the functional microsphere in vivo. Single photo emission computed tomography (SPECT) imaging was used to monitor ^{177}Lu-MS@PDA microspheres in vivo after TARE. It was demonstrated that TARE/PTT-combined therapy enabled by the dual-functional ^{177}Lu-MS@PDA can significantly inhibit the growth of HCC without inducing obvious side effects.

Scheme 1. Preparation of Polydopamine-Coated Silica Microspheres Pre-Labeled with ^{177}Lu for TARE/PTT of Hepatocellular Carcinoma

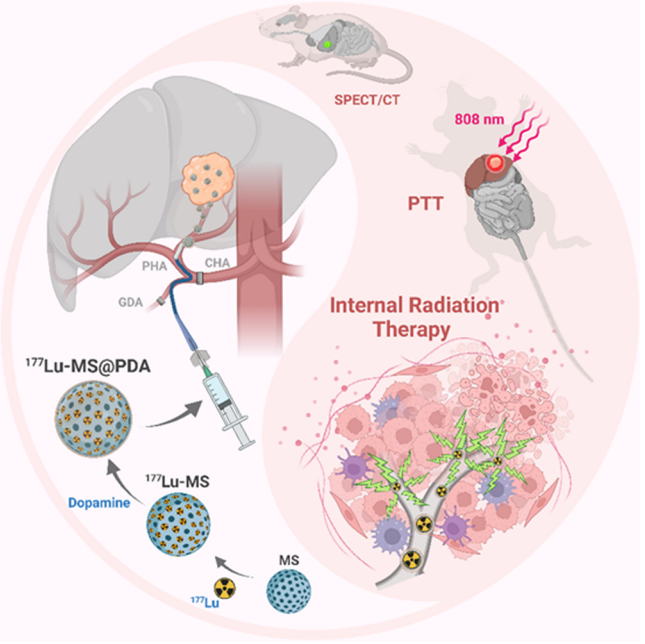

EXPERIMENTAL SECTION

Chemicals. $^{177}LuCl_3$ was purchased from China Isotope & Radiation Corporation. Silica microspheres (MS) were purchased from Suzhou Knowledge & Benefit Sphere Tech. Co., Ltd. All other reagents were commercially available products and used as received without further purification.

Preparation and Characterization of ^{177}Lu-MS@PDA. The ^{177}Lu-labeled silica microspheres (MS) were prepared according to a previous report[24] and denoted as ^{177}Lu-MS. Briefly, $^{177}LuCl_3$ solution (5 μL, 100 μCi) was added into 0.5 mL of H_2O containing 10 mg of silica MS. After 2 min under shaking at 25 °C, 100 μL of aqueous solution of K_3PO_4 (1 M) was introduced into the above solution. ^{177}Lu-MS were collected by centrifugation. After rinsing with pure water, the resulting ^{177}Lu-MS were dispersed in 1 mL of Tris buffer (pH 8.5) containing 4 mg of dopamine hydrochloride. After incubation for 30 min at 25 °C under shaking, the final product was collected and purified to obtain PDA-coated ^{177}Lu-MS, denoted as ^{177}Lu-MS@PDA.

Radioactivity was measured by a dose calibrator (Capintec, CRC-25R, USA). For characterization, non-radioactive MS@PDA were prepared according to the same method mentioned above and used as control. The size and morphology of mother MS and MS@PDA were characterized using an optical microscope (Olympus, IX73, Japan) and a scanning electron microscope (Zeiss, EVO 18, Germany), respectively. X-ray photoelectron spectroscopy (Thermo Scientific, Escalab 250Xi, Japan) equipped with a monochromatic Al Kα X-ray source (1486.6 eV) operating at 100 W was used to analyze the surface chemistry of MS@PDA and MS. All peaks were calibrated with C 1s peak binding energy at 284.8 eV for adventitious carbon. The infrared spectra of MS@PDA and other substances were obtained using a Fourier transform infrared spectrophotometer (Bruker, VERTEX 70, Germany) from 600 to 4000 cm^{-1} at room temperature. To assess the optical properties, the absorption of Lu-MS@PDA was recorded on a UV−VIS−NIR (Persee, TU1901, China). The content of PDA coated on MS was quantified using a thermogravimetric analyzer (Netzsch, STA 449 F3, Germany) from 30 to 900 °C with a heating rate of 15 °C min^{-1} under a nitrogen atmosphere with flow of 50 mL min^{-1}.

Radiostability of ^{177}Lu-MS@PDA. The radiostability of ^{177}Lu-MS@PDA was evaluated in different solutions including saline and 10% fetal bovine serum (FBS) at room temperature. The supernatants collected at 0, 2, 4, 24, 48, and 96 h were measured by the gamma counter. In the same way, the radiostability of ^{177}Lu-MS and ^{177}Lu-MS@PDA after 808 nm NIR laser irradiation at a power density of 1.5 W/cm^2 for 5 min was determined to show the stabilizing effect of PDA for the surface-labeled ^{177}Lu.

In Vitro Photothermal Performance of PDA Coating on Microspheres. The photothermal performance of PDA-coated microspheres was evaluated under 808 nm NIR laser irradiation (Hi-Tech Optoelectronics Co., Ltd., Beijing, China). Real-time thermal images were acquired with an infrared camera (FLIR, Ax5

https://doi.org/10.1021/acsami.2c19829
ACS Appl. Mater. Interfaces XXXX, XXX, XXX−XXX

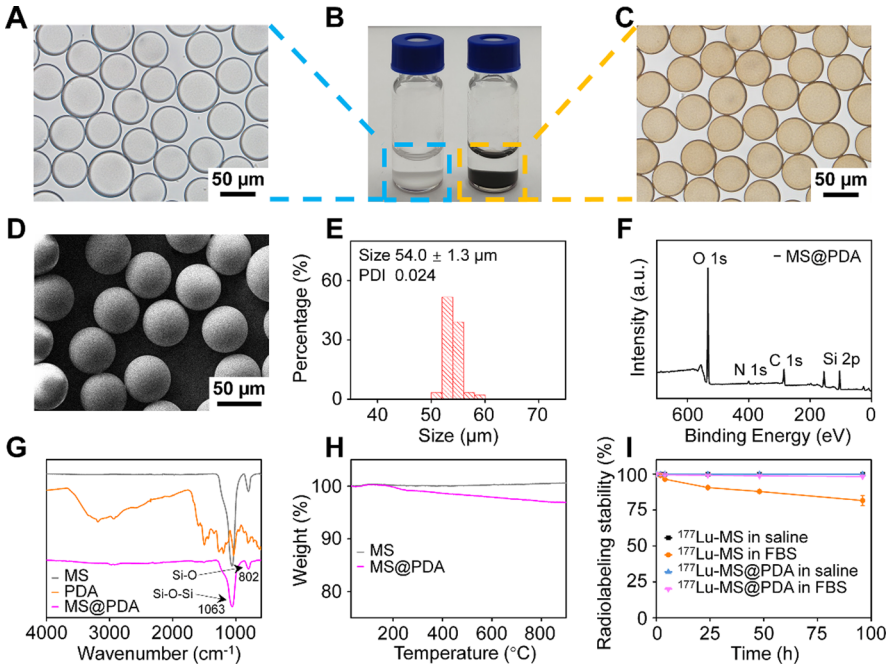

Figure 1. (A) Optical microscope image of the mother silica microspheres (MS). (B) Photograph of suspensions of MS (left) and MS@PDA (right). (C) Optical microscope image of MS@PDA. (D, E) SEM image and histogram of MS@PDA. (F) XPS spectrum of MS@PDA. (G) FTIR spectra of MS@PDA, MS, and PDA. (H) TG curves of MS@PDA and MS. (I) Radiostability of ^{177}Lu-MS and ^{177}Lu-MS@PDA in saline and 10% FBS, respectively.

Series, USA) during irradiation. In detail, 1 mL aqueous solutions containing 8 mg of MS or MS@PDA were irradiated at a power density of 1.5 W/cm^2 for 10 min. To evaluate the concentration effect, the above MS@PDA solutions were further diluted by two-, four-, and eightfold, respectively. Under the same experimental conditions, the photothermal effects were recorded and compared. In addition, varied laser power densities, e.g., 0.5, 1.0, 1.5, and 2.0 W/cm^2, were applied to evaluate the power density-dependent photothermal conversion effects of MS@PDA (8 mg/mL). The illumination time was 5 min alternated by natural cooling of 1 mL suspension of MS@PDA to room temperature, and the on/off cycle was repeated for five times.

Cytotoxicity Assay. The methyl thiazolyl tetrazolium (MTT) assay was adopted to evaluate the potential cytotoxicity of MS@PDA. N1S1 rat hepatoma cells and 3T3 mouse embryonic fibroblast cells were cultured in DMEM containing 10% FBS and 1% antibiotics at 37 °C in an atmosphere containing 5% CO_2, respectively, and they were inoculated in a 96-well plate by approximately 1 × 10^4 cells per well and cultured for 12 h to make the cells adherent. Afterward, the N1S1 cells and 3T3 cells were incubated for 12 h with MS@PDA at different concentrations, i.e., 0, 62.5, 125, 250, and 500 μg/mL, respectively. After the cells were rinsed with PBS, 100 μL of MTT solution was added to the 96-well plate and maintained there for 4 h. Then, DMSO was added after MTT was removed for detecting the absorbance of each well with a multi-function microplate reader (Thermo Scientific, Varioskan Flash, Japan).

In addition, the N1S1 cells were inoculated in the 96-well plate according to the same conditions as above, and then subjected to the following treatments, i.e., saline (control group), MS@PDA (500 μg/mL), MS@PDA (500 μg/mL) following laser irradiation for 5 min, ^{177}Lu-MS@PDA (500 μg/mL, 50 μCi), and ^{177}Lu-MS@PDA (500 μg/mL, 50 μCi) following laser irradiation for 5 min, and then continued to incubate for 24 h, and the subsequent MTT assay was the same as above.

Immunofluorescence Cell Assay. The N1S1 cells were inoculated in cell slides with about 2.5 × 10^5 cells per slide for 12 h and then subjected to treatments with saline (control group), MS@PDA (500 μg/mL), MS@PDA (500 μg/mL), ^{177}Lu-MS@PDA (500 μg/mL, 200 μCi), and ^{177}Lu-MS@PDA (500 μg/mL, 200 μCi), respectively, under laser irradiation for 5 min, followed by 24 h incubation. After that, the cells were fixed with 4% paraformaldehyde for 15 min. Triton X-100 (0.5%) was introduced to improve the permeability of the cell membrane through incubation of approximately 15 min. Then, the cells obtained were immersed in a blocking buffer (5% bovine serum albumin in Tris-buffered saline solution) for 1 h at 37 °C. Afterward, the cells were incubated with anti-histone γ-H2AX mouse monoclonal antibodies for 2 h at 37 °C and then incubated with a rabbit anti-mouse secondary antibody for 1 h at 37 °C in the dark. The resulting cell nuclei were stained with Hoechst (20 μL, 5 mg/mL) for 5 min. Fluorescence images were obtained on a confocal laser scanning microscope (CLSM, Olympus FV1200, Japan).

Animal Experiments. Sprague−Dawley rats (male, 9−11 weeks of age) of specific pathogen-free grade were purchased from Beijing Vital River Laboratory Animal Technology Co., Ltd. The orthotopic HCC tumor model was established by injection of N1S1 cells into the rat liver anesthetized with chloral hydrate delivered through intraperitoneal injection (400 mg/kg body weight). Then, the abdomen of rats was cut along the midline to expose the left liver lobe for the injection of 50 μL of N1S1 cells (1 × 10^7). Finally, the abdominal cavity was sutured. Magnetic resonance imaging (MRI, GE, SIGNA Architect, USA) was used to monitor the tumor growth. In vivo biodistribution and anti-tumor study were conducted when the tumor volume reached 200 mm^3.

For arterial cannulation, the abdomen was opened following the protocol mentioned above. Then, proper hepatic (PHA), gastroduodenal (GDA), and common hepatic arteries (CHA) were exposed. The distal end of the GDA and the CHA were temporarily ligated, and a catheter was placed into the PHA from upstream of the GDA distal ligature. Microspheres were administered through the catheter. Finally, the hepatic arterial flow was restored and the abdominal cavity was sutured. 5 mg of MS@PDA was injected into PHA, and the rats were sacrificed 3 days later. The tumors were dissected for histochemical analysis through hematoxylin & eosin (H&E) staining.

Photothermal Imaging of MS@PDA In Vivo. To evaluate the photothermal conversion effects of MS@PDA in vivo, 5 mg of MS@PDA was injected into PHA through arterial cannulation. The tumor

https://doi.org/10.1021/acsami.2c19829
ACS Appl. Mater. Interfaces XXXX, XXX, XXX−XXX

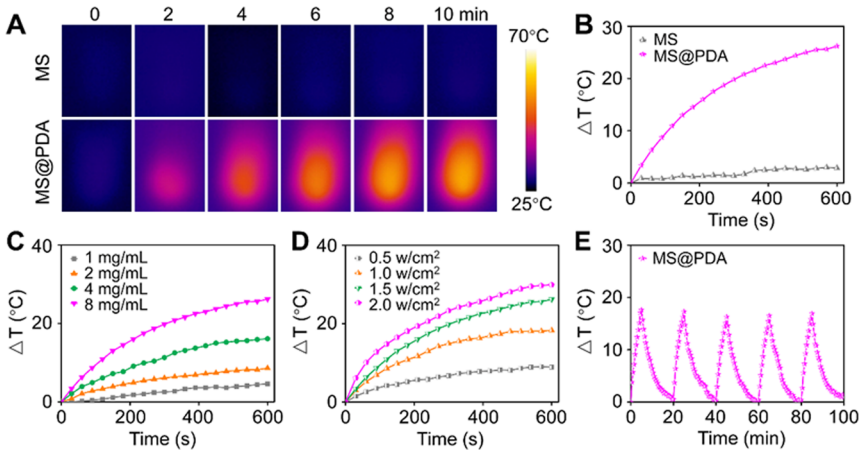

Figure 2. (A, B) Photothermal effects of MS and MS@PDA (8 mg/mL) recorded during laser irradiation with an 808 nm laser (1.5 W/cm^2). (C, D) Temporal temperatures increasing the effect of MS@PDA with concentrations of 1, 2, 4, and 8 mg/mL for comparing with MS@PDA (8 mg/mL) with different irradiation powers of 0.5, 1.0, 1.5, and 2 W/cm^2. (E) Photothermal stabilities of MS@PDA at 8 mg/mL over five laser on/off cycles (808 nm, 1.5 W/cm^2).

was irradiated by the 808 nm NIR laser at a power density of 1.5 W/cm^2 for 5 min, and real-time thermal images were recorded with an infrared camera.

Radiostability of ^{177}Lu-MS@PDA In Vivo. To evaluate the radiostability of ^{177}Lu-MS@PDA in vivo, N1S1 orthotopic tumor-bearing rats were injected with ^{177}Lu-MS@PDA (5 mg, 500 μCi) through arterial cannulation. After injection of ^{177}Lu-MS@PDA, the blood sample was drawn from the retinal vein at days 3, 7, and 14 days for radioactivity assay by the gamma counter.

MicroSPECT/CT Imaging of ^{177}Lu-MS@PDA In Vivo. N1S1 tumor-bearing rats were injected with ^{177}Lu-MS@PDA (5 mg, 800 μCi) through PHA and in vivo imaging was carried out a MicroSPECT/CT (MILabs, U-SPECT$^+$, the Netherlands) at 1 h, 1 day, 4 days, 8 days, 16 days, and 32 days, respectively, post-injection. The scan rate was set as 10 min/frame. The CT scanning was carried out by precise mode with all-angle, three-frame average, 615 mA tube current, and 55 kV tube voltage. The MicroSPECT/CT images were analyzed with PMOD software (version 3.602). To show the biodistribution of ^{177}Lu-MS@PDA, the rats were dissected after the imaging experiments. The weight and radioactivity of major organs and tumors were measured and analyzed.

Inhibition of Tumor Growth In Vivo. To evaluate the tumor inhibition effect, orthotopic N1S1 tumor-bearing rats (200−300 mm^3) were randomly divided into five groups and then subjected to treatments through arterial cannulation with saline (control), MS@PDA (5 mg), MS@PDA (5 mg), ^{177}Lu-MS@PDA (5 mg, 500 μCi), and ^{177}Lu-MS@PDA (5 mg, 500 μCi), respectively, following laser irradiation of 1.5 W/cm^2 for 5 min. The tumor volume was monitored by MRI. The bio-safety of the radioactive microspheres was assessed through the expression levels of liver enzymes including alanine aminotransferase (ALT), aspartate aminotransferase (AST), alkaline phosphatase (ALP), and gamma glutamyl transpeptidase (GGT). Blood samples were collected on days 0, 3, 7, and 14 post-treatment, respectively. Meanwhile, the body weights of the rats were recorded. All rats were sacrificed on day 14 post-treatment. The tumor and major organs were harvested for histochemical analysis through H&E staining. In addition, the tumor slices were analyzed by terminal deoxynucleotidyl transferase dUTP nick end labeling (TUNEL) assay.

RESULTS AND DISCUSSION

Preparation and Characterization of ^{177}Lu-MS@PDA. ^{177}Lu-MS with high radiolabeling efficiency (97.8 ± 1.2%) were obtained through a facile precipitating method, as previously reported.[24] ^{177}Lu-MS@PDA were prepared by coating ^{177}Lu-MS with PDA. The non-radioactive MS@PDA were fully characterized instead of ^{177}Lu-MS as the latter require complicated radiation protection. As shown in Figure 1A−C, the optical microscopy images and photography reveal that MS@PDA are in perfect spherical shape with uniform size and brown color after PDA coating. Dopamine is oxidized and polymerized in a weak base environment containing oxygen. It can be attached to the surface of various organic or inorganic materials to form PDA coating.[44] Further, the scanning electron microscopy (SEM) results confirm that PDA coating does not change the morphology of mother MS (Figure 1D and Figure S1A). According to the optical imaging results, the average size of MS@PDA is around 54.0 ± 1.3 μm with a polydispersity index of 0.024, as given in Figure 1E. The size and size distribution of MS@PDA were slightly increased upon PDA coating (Figure S1B). The XPS studies support the presence of nitrogen in microspheres obtained after PDA coating according to the binding energy peak appearing at 400 eV (Figure 1F and Figure S2). Meanwhile, the Fourier transform infrared (FTIR) spectrum of MS@PDA displays strong vibrational absorption bands at 1063 cm^{-1} (Si−O−Si vibration mode) and 802 cm^{-1} (Si−O vibration mode), respectively, contrasting to that for MS, which also supports successful PDA coating on the surface of MS (Figure 1G). In addition, thermogravimetric analysis (TGA) was carried out to investigate the composition of MS@PDA. According to the TGA curve in Figure 1H, the weight loss of MS@PDA at 900 °C is around 3% corresponding to the 500 nm thick PDA film evenly coated on MS. UV absorption of ^{177}Lu-MS@PDA was tested, and the results in Figure S3 showed that ^{177}Lu-MS@PDA exhibited broad absorption.

The radiostability of ^{177}Lu-MS and ^{177}Lu-MS@PDA in saline and 10% fetal bovine serum (FBS) was tested at room temperature. Both of ^{177}Lu-MS and ^{177}Lu-MS@PDA are quite stable in saline. However, 20% of free ^{177}Lu was detected in solution after ^{177}Lu-MS were incubated within 10% FBS. In contrast, this number dropped to less than 2% after ^{177}Lu-MS were coated with PDA (Figure 1I), demonstrating that the PDA coating can significantly improve the radiostability of the ^{177}Lu-labeled silica microspheres by firmly gluing the silica sphere and ^{177}Lu together, which also endows the resulting microspheres with photothermal therapeutic functions. In addition, ^{177}Lu-MS@PDA maintained good radiostability after 808 nm laser irradiation, which proves that laser stimulation

https://doi.org/10.1021/acsami.2c19829
ACS Appl. Mater. Interfaces XXXX, XXX, XXX−XXX

does not affect the radiostability of ^{177}Lu-MS@PDA (Figure S4).

Photothermal Performance of PDA-Coated MS In Vitro. The photothermal performance of MS@PDA was evaluated in vitro upon irradiation with the 808 nm laser. As shown in Figure 2A,B, the temperature of the MS@PDA suspension (8 mg/mL) is increased by 26 °C after irradiation of 10 min with a power density of 1.5 W/cm^2. In comparison, the temperature of the suspension of the mother MS only increases by 3 °C, clearly verifying the outstanding photothermal conversion effect of PDA. In addition, we measured the photothermal conversion efficiency (η) of MS@PDA. The η value was calculated as follows and determined to be 42%.

$$\eta = \frac{hA(\Delta T_{\max,\text{sample}} - \Delta T_{\max,\text{solvent}})}{I(1 - 10^{-\text{A808}})}$$

where h is the heat transfer coefficient, A is the surface area of the container, $\Delta T_{\max,\text{sample}}$ is the temperature change of the ^{177}Lu-MS@PDA solution, $\Delta T_{\max,\text{solvent}}$ is the temperature change of solvent, I is the laser power, and A808 is the absorbance of ^{177}Lu-MS@PDA solution at 808 nm.

As shown in Figure 2C,D, the photothermal performance of MS@PDA is positively correlated with both concentration of the microspheres and the power density of the incident laser as well. For example, the temperature of the MS@PDA suspension (8 mg/mL) was increased by 9, 18, 26, and 30 °C upon 10 min irradiation at power densities of 0.5, 1.0, 1.5, and 2.0 W/cm^2, respectively (Figure 2D), which demonstrates the excellent hyperthermia effects of PDA-coated MS for killing tumor cells. In addition, the highly reproducible on/off cycles, as shown in Figure 2E, not only reveal an outstanding photothermal stability of the PDA-coated microspheres but also indicate that the current microspheres can potentially be used for multiple-shot PTT of tumors analogous to tumor radiofrequency ablation.

Cytotoxicity and Mechanism of Combinatorial Therapy. Prior to the in vivo study, the cytotoxicity of ^{177}Lu-MS@PDA on N1S1 cells was evaluated. After incubation for 24 h with ^{177}Lu-MS@PDA followed by laser irradiation of 5 min at 808 nm, the cell viability was remarkably decreased to 22.9 ± 3.2%, as shown in Figure 3A. Further, the immunofluorescence assay confirms that the heaviest DNA damage is induced by the combination of radiation and thermal therapies (Figure 3B,C). In addition, the cytotoxicity of MS@PDA on both 3T3 and N1S1 cells was also investigated. From the results of the MTT assay shown in Figure S5, the cell viability remained as high as >90% even when the MS@PDA concentration was of 500 μg/mL, indicating that MS@PDA possesses excellent biosafety. The above results not only demonstrate that PDA-coated microspheres have good biocompatibility but also imply that ^{177}Lu-MS@PDA can excellently internal radiation therapy with PTT.

To investigate the mechanism of the combination therapy, flow cytometry analysis was carried out on N1S1 cells with different treatments. As well known, the G2/M phase is the cell cycle with the highest radiosensitivity. Compared with the control group (G2/M: 16.3 ± 1.7%), PTT caused G2/M arrest and increased the ratio of G2/M phase cells (G2/M: 22.0 ± 1.2%). The low dose of the ^{177}Lu-MS@PDA group had little effect on the cycle arrest (G2/M: 15.1 ± 5.8%), but photothermal therapy caused the rise of G2/M phase cells, which can increase the radiation sensitivity of the cell

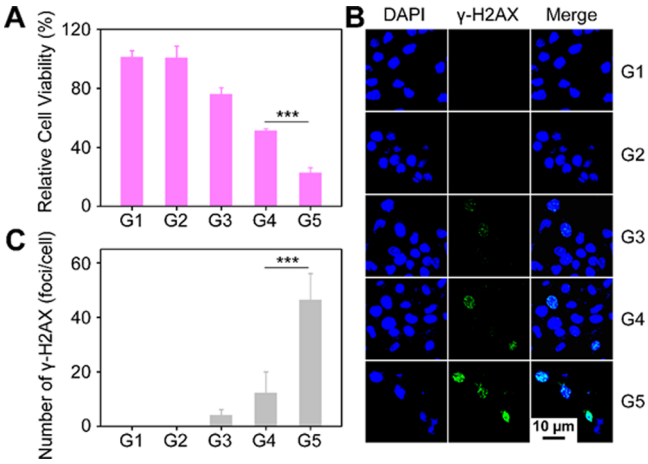

Figure 3. (A, B) Relative viability and immunofluorescence assays of N1S1 cells recorded for different treatments, respectively. (C) Quantification of cellular γ-H2AX foci densities of the fluorescence images (G1: control; G2: MS@PDA; G3: MS@PDA + laser; G4: ^{177}Lu-MS@PDA; G5: ^{177}Lu-MS@PDA + laser). P values were calculated by one-way ANOVA with Tukey multiple-comparison tests, ***P < 0.001.

population (G2/M: 26 ± 2.5%) (Figure S6). Therefore, the increased proportion of G2/M phase cells caused by PTT and radiation of ^{177}Lu enhanced the overall radiosensitivity, so the tumor cells were killed by PTT and radiation of ^{177}Lu, resulting in a synergistic effect.

Theranostic Functions of ^{177}Lu-MS@PDA In Vivo. Arterial cannulation of orthotopic HCC tumors in rats has been widely used for embolization studies.[45,46] The orthotopic HCC tumor model was constructed by injecting N1S1 cells into the rat liver. When the tumor volume reached around 200 mm^3 monitored by MRI, the rats were ready for the subsequent experiments. The microspheres were administered through hepatic artery cannulation; the procedures are shown in Figure S7A. H&E staining of the tumor slice confirms that MS@PDA were successfully delivered into the blood vessels of the tumor (Figure S7B), confirming that arterial cannulation administration of MS@PDA is reliable for animal experiments.

An in vivo photothermal conversion experiment was performed on rats bearing N1S1 orthotopic HCC tumors after MS@PDA was delivered through hepatic artery cannulation. Irradiation of 5 min with the 808 nm laser at a power density of 1.5 W/cm^2 can increase the local temperature of the tumor site by more than 12 °C (Figure 4A,B). This result illustrates well the excellent photothermal conversion effect of MS@PDA in vivo.

To evaluate the radiostability of ^{177}Lu-MS@PDA in vivo, N1S1 orthotopic tumor-bearing rats were injected with ^{177}Lu-MS@PDA (5 mg, 500 μCi) through arterial cannulation and the blood sample was drawn from the retinal vein at days 3, 7, and 14 for the radioactivity assay. The results in Figure S8 showed that less than 0.010 %ID/g of ^{177}Lu was detected in the blood, demonstrating that ^{177}Lu-MS@PDA has high radiostability in vivo.

The biodistribution of ^{177}Lu-MS@PDA in rats bearing N1S1 orthotopic HCC tumors was monitored by MicroSPECT/CT. After hepatic intra-arterial administration, SPECT/CT scans were conducted at different time points post-injection. The images of SPECT show that the radioactive signal of ^{177}Lu remains detectable 32 days post-injection and no obvious

https://doi.org/10.1021/acsami.2c19829
ACS Appl. Mater. Interfaces XXXX, XXX, XXX−XXX

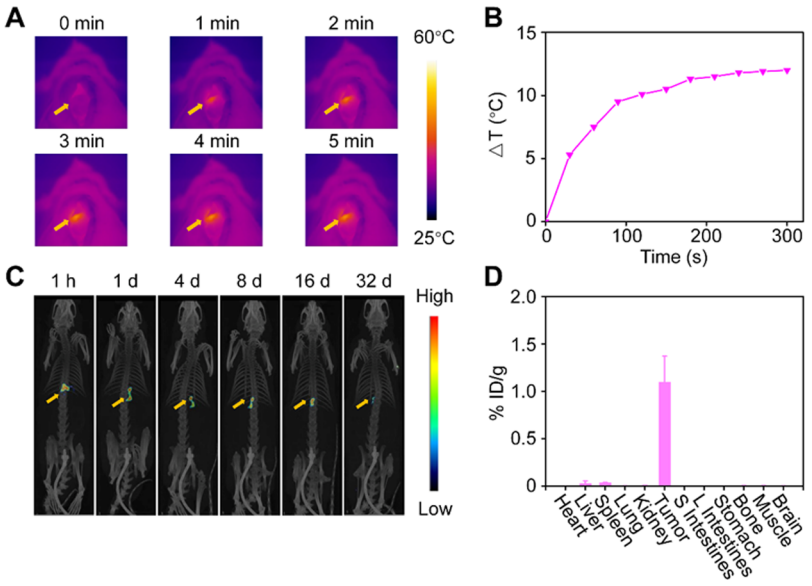

Figure 4. (A, B) Photothermal images and temperature of the tumor site injected with MS@PDA followed by laser treatment (n = 3). (C) SPECT/CT images of N1S1 tumor-bearing rats injected with ^{177}Lu-MS@PDA. (D) Biodistribution of ^{177}Lu obtained on day 32 after administration.

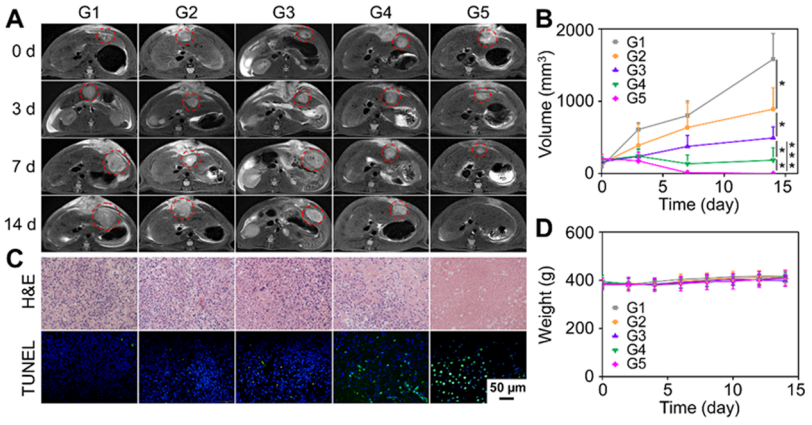

Figure 5. (A, B) T_2-weighted MR images of tumors highlighted with red dashed circles together with the temporal tumor volume recorded after different treatments (n = 5). (C) Macroscopic images of N1S1 tumor slices obtained 14 days post-treatment and stained with H&E and TUNEL, respectively. (D) Body weight of N1S1 tumor-bearing rats receiving different treatments (G1: control; G2: MS@PDA; G3: MS@PDA + laser; G4: ^{177}Lu-MS@PDA; G5: ^{177}Lu-MS@PDA + laser). P values were calculated by one-way ANOVA with Tukey multiple-comparison tests, *P < 0.05, **P < 0.01, and ***P < 0.001.

radioactive signal is found in other organs or tissues (Figure 4C), further indicating that ^{177}Lu-MS@PDA embolized in HCC have excellent radiostability in vivo. The rats were sacrificed after imaging experiments, and the radioactivity of major organs and tumors were measured by a gamma counter. The biodistribution results in Figure 4D show that ^{177}Lu-MS@PDA are mainly accumulated in the tumor (1.10 ± 0.27 %ID/g), showing a long-time retention of ^{177}Lu-MS@PDA in the tumor. A small amount of radioactivity appeared in the liver (0.03 ± 0.03 %ID/g) and spleen (0.04 ± 0.01 %ID/g), which might be caused by ectopic embolization, while no obvious radioactivity was found in other major organs. All the above results suggest that ^{177}Lu-MS@PDA hold great potential for HCC radioembolization and nuclear imaging.

Tumor Growth Inhibition In Vivo. The tumor-therapeutic effect of ^{177}Lu-MS@PDA was evaluated on rats bearing N1S1 orthotopic HCC tumors by hepatic artery cannulation administration, and MRI was carried out on days 0, 3, 7, and 14, respectively, to monitor the volume of tumors. The tumor-bearing rats were randomly divided into five groups and received saline, MS@PDA, MS@PDA plus 300 s laser irradiation, ^{177}Lu-MS@PDA (500 μCi), and ^{177}Lu-MS@PDA (500 μCi) plus 300 s laser irradiation, respectively. From the MR images of tumor-bearing rats (Figure 5A,B) acquired before and after the above treatment, it is found that ^{177}Lu-MS@PDA plus laser treatment can significantly inhibit the tumor growth, indicating that radioembolization combined with PTT can effectively treat the HCC. Meanwhile, the treatment does not lead to obvious loss of body weight of rats (Figure 5D), demonstrating that ^{177}Lu-MS@PDA combined with PTT has no obvious side effects. In addition, the biosafety of ^{177}Lu-MS@PDA was evaluated through expression levels of liver enzymes, i.e., ALT, AST, ALP, and GGT. As shown in Figure S9, the levels of liver enzymes increases after treatment with ^{177}Lu-MS@PDA followed by PTT, which might be affected by the surgical procedure,[47] but they

https://doi.org/10.1021/acsami.2c19829
ACS Appl. Mater. Interfaces XXXX, XXX, XXX−XXX

returned to normal within 2 weeks, suggesting that the combined treatment is safe. According to the ethical rules, the rats were sacrificed when the tumor volume of the control group reached 1500 mm^3. The tumors and major organs were harvested, sliced, and then subjected to H&E and TUNEL staining. As shown in Figure 5C, the microscopy images show that ^{177}Lu-MS@PDA plus laser treatment gives rise to remarkable necrosis and apoptosis compared to other groups. Meanwhile, H&E staining of major organs does not show obvious damage (Figure 6), which also demonstrates the safeness of ^{177}Lu-MS@PDA treatment in combination with PTT.

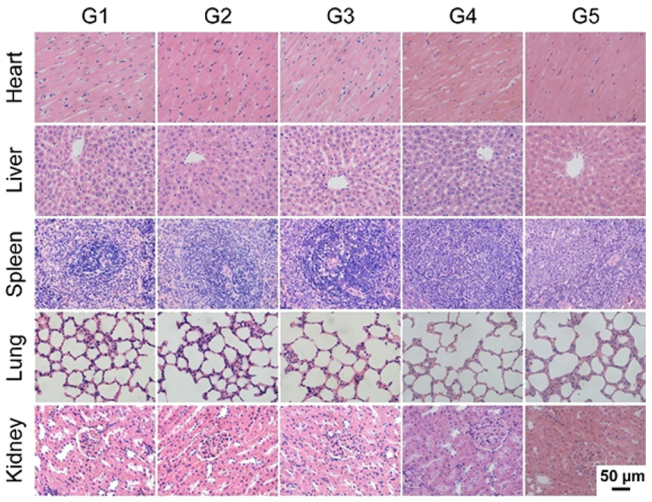

Figure 6. Macroscopic H&E staining images of different organs of N1S1 tumor-bearing rats harvested 14 days post-treatment (G1: control; G2: MS@PDA; G3: MS@PDA + laser; G4: ^{177}Lu-MS@PDA; G5: ^{177}Lu-MS@PDA + laser).

CONCLUSIONS

In summary, we have prepared a novel ^{177}Lu-MS@PDA for TARE/PTT combinatorial therapy. The radiostability of ^{177}Lu-MS@PDA is significantly improved by coating the mother ^{177}Lu-MS with PDA. MicroSPECT/CT imaging studies demonstrate the long-time retention and excellent radiostability of ^{177}Lu-MS@PDA in vivo. The therapeutic efficacy and bio-safety studies suggest that ^{177}Lu-MS@PDA combined with PTT can effectively inhibit the tumor growth without inducing obvious side effects. This new multifunctional microsphere can be applied in TARE/PTT of HCC. Hepatic artery embolization can accurately deliver the microsphere to the tumor site, and the application of photothermal treatment can reduce the radiation dose and improve the therapeutic effect. Therefore, ^{177}Lu-MS@PDA provides a promising radioactive microsphere for clinical treatment of HCC.

ASSOCIATED CONTENT

Supporting Information

The Supporting Information is available free of charge at https://pubs.acs.org/doi/10.1021/acsami.2c19829.

TEM and size distribution, XPS data, UV absorption, radiostability, cell viability data, hepatic artery cannulation and H&E staining data, radioactivity in blood, and expression levels of liver enzymes (PDF)

AUTHOR INFORMATION

Corresponding Authors

Guanglin Wang − *State Key Laboratory of Radiation Medicine and Protection, School of Radiation Medicine and Protection, Collaborative Innovation Center of Radiation Medicine of Jiangsu Higher Education Institutions, Soochow University, Suzhou 215123, China*; orcid.org/0000-0002-6463-119X; Email: glwang@suda.edu.cn

Mingyuan Gao − *State Key Laboratory of Radiation Medicine and Protection, School of Radiation Medicine and Protection, Collaborative Innovation Center of Radiation Medicine of Jiangsu Higher Education Institutions, Soochow University, Suzhou 215123, China*; Email: gaomy@iccas.ac.cn

Authors

Manran Wu − *State Key Laboratory of Radiation Medicine and Protection, School of Radiation Medicine and Protection, Collaborative Innovation Center of Radiation Medicine of Jiangsu Higher Education Institutions, Soochow University, Suzhou 215123, China*

Lei Zhang − *Department of Interventional Radiology, The First Affiliated Hospital of Soochow University, Suzhou 215006, China*

Kexin Shi − *State Key Laboratory of Radiation Medicine and Protection, School of Radiation Medicine and Protection, Collaborative Innovation Center of Radiation Medicine of Jiangsu Higher Education Institutions, Soochow University, Suzhou 215123, China*

Dongxu Zhao − *Department of Interventional Radiology, The First Affiliated Hospital of Soochow University, Suzhou 215006, China*

Weipeng Yong − *State Key Laboratory of Radiation Medicine and Protection, School of Radiation Medicine and Protection, Collaborative Innovation Center of Radiation Medicine of Jiangsu Higher Education Institutions, Soochow University, Suzhou 215123, China*

Lingling Yin − *State Key Laboratory of Radiation Medicine and Protection, School of Radiation Medicine and Protection, Collaborative Innovation Center of Radiation Medicine of Jiangsu Higher Education Institutions, Soochow University, Suzhou 215123, China*

Ruizhe Huang − *State Key Laboratory of Radiation Medicine and Protection, School of Radiation Medicine and Protection, Collaborative Innovation Center of Radiation Medicine of Jiangsu Higher Education Institutions, Soochow University, Suzhou 215123, China*

Gang Huang − *Shanghai Key Laboratory of Molecular Imaging, Shanghai University of Medicine and Health Sciences, Shanghai 201318, China*

Complete contact information is available at: https://pubs.acs.org/10.1021/acsami.2c19829

Author Contributions

#M.W., L.Z., and K.S. contributed equally. The manuscript was written through contributions of all authors. All authors have given approval to the final version of the manuscript.

Notes

The authors declare no competing financial interest.

All animal experiment protocols were followed by the Animal Ethics Committee of the Soochow University Laboratory Animal Center (approval number: 202007A554.)

https://doi.org/10.1021/acsami.2c19829
ACS Appl. Mater. Interfaces XXXX, XXX, XXX−XXX

■ ACKNOWLEDGMENTS

The authors thank the financial support from the National Natural Science Found of China (81720108024, 21976128, and 82130059), the National Key Research Program of China (2018YFA0208800), and Priority Academic Program Development of Jiangsu Higher Education Institutions (PAPD). G.W. thanks the support from the Natural Science Foundation of Jiangsu Province (BK20200100) and the Undergraduate Training Program for Innovation and Entrepreneurship Soochow University (202010285046Z).

■ REFERENCES

(1) Sung, H.; Ferlay, J.; Siegel, R. L.; Laversanne, M.; Soerjomataram, I.; Jemal, A.; Bray, F. Global Cancer Statistics 2020: GLOBOCAN Estimates of Incidence and Mortality Worldwide for 36 Cancers in 185 Countries. *CA Cancer J. Clin.* **2021**, *71*, 209−249.

(2) Yang, J. D.; Hainaut, P.; Gores, G. J.; Amadou, A.; Plymoth, A.; Roberts, L. R. A global View of Hepatocellular Carcinoma: Trends, Risk, Prevention and Management. *Nat. Rev. Gastroenterol. Hepatol.* **2019**, *16*, 589−604.

(3) Daher, S.; Massarwa, M.; Benson, A. A.; Khoury, T. Current and Future Treatment of Hepatocellular Carcinoma: An Updated Comprehensive Review. *J. Clin. Transl. Hepatol.* **2018**, *6*, 69−78.

(4) Morise, Z.; Kawabe, N.; Tomishige, H.; Nagata, H.; Kawase, J.; Arakawa, S.; Yoshida, R.; Isetani, M. Recent Advances in the Surgical Treatment of Hepatocellular Carcinoma. *World J. Gastroenterol.* **2014**, *20*, 14381−14392.

(5) Dutta, R.; Mahato, R. I. Recent Advances in Hepatocellular Carcinoma Therapy. *Pharmacol. Ther.* **2017**, *173*, 106−117.

(6) Jiang, Y.; Sun, A. H.; Zhao, Y.; Ying, W. T.; Sun, H. C.; Yang, X. R.; Xing, B. C.; Sun, W.; Ren, L. L.; Hu, B.; Li, C. Y.; Zhang, L.; Qin, G. R.; Zhang, M. H.; Chen, N.; Zhang, M. L.; Huang, Y.; Zhou, J. N.; Zhao, Y.; Liu, M. W.; Zhu, X. D.; Qiu, Y.; Sun, Y. J.; Huang, C.; Yan, M.; Wang, M. C.; Liu, W.; Tian, F.; Xu, H. L.; Zhou, J.; Wu, Z. Y.; Shi, T. L.; Zhu, W. M.; Qin, J.; Xie, L.; Fan, J.; Qian, X. H.; He, F. C.; Zhu, Y. P.; Wang, Y.; Yang, D.; Liu, W. L.; Liu, Q. M.; Yang, X. M.; Zhen, B.; Wu, Z. Y.; Fan, J.; Sun, H. C.; Qian, J. Y.; Hong, T.; Shen, L.; Xing, B. C.; Yang, P. Y.; Shen, H. L.; Zhang, L. J.; Cheng, S. J.; Cai, J. Q.; Zhao, X. H.; Sun, Y. L.; Xiao, T.; Mao, Y. S.; Chen, X. M.; Wu, D.; Chen, L.; Dong, J.; Deng, H. T.; Tan, M. J.; Wu, Z. X.; Zhao, Q. C.; Shen, Z. Y.; Chen, X. G.; Gao, Y. H.; Sun, W.; Wang, T.; Liu, S. Q.; Lin, L.; Zi, J.; Lou, X. M.; Zeng, R.; Wu, Y.; Cai, S. J.; Jiang, B.; Chen, A. Q.; Li, Z. J.; Yang, F. Q.; Chen, X. L.; Sun, Y. N.; Wang, Q. L.; Zhang, Y.; Wang, G. S.; Chen, Z. C.; Qin, W. S.; Li, Z. S.; Chinese Human Proteome Project, C. Proteomics Identifies New Therapeutic Targets of Early-Stage Hepatocellular Carcinoma. *Nature* **2019**, *567*, 257−261.

(7) Edeline, J.; Touchefeu, Y.; Guiu, B.; Farge, O.; Tougeron, D.; Baumgaertner, I.; Ayav, A.; Campillo-Gimenez, B.; Beuzit, L.; Pracht, M.; Lièvre, A.; Le Sourd, S.; Boudjema, K.; Rolland, Y.; Boucher, E.; Garin, E. Radioembolization Plus Chemotherapy for First-Line Treatment of Locally Advanced Intrahepatic Cholangiocarcinoma A Phase 2 Clinical Trial. *JAMA Oncol.* **2020**, *6*, 51−59.

(8) Lee, E. W.; Khan, S. Recent Advances in Transarterial Embolotherapies in the Treatment of Hepatocellular Carcinoma. *Clin. Mol. Hepatol.* **2017**, *23*, 265−272.

(9) Brown, K. T.; Do, R. K.; Gonen, M.; Covey, A. M.; Getrajdman, G. I.; Sofocleous, C. T.; Jarnagin, W. R.; D'Angelica, M. I.; Allen, P. J.; Erinjeri, J. P.; Brody, L. A.; O'Neill, G. P.; Johnson, K. N.; Garcia, A. R.; Beattie, C.; Zhao, B. S.; Solomon, S. B.; Schwartz, L. H.; DeMatteo, R.; Abou-Alfa, G. K. Randomized Trial of Hepatic Artery Embolization for Hepatocellular Carcinoma Using Doxorubicin-Eluting Microspheres Compared with Embolization with Microspheres Alone. *J. Clin. Oncol.* **2016**, *34*, 2046−2053.

(10) Weber, M.; Lam, M.; Chiesa, C.; Konijnenberg, M.; Cremonesi, M.; Flamen, P.; Gnesin, S.; Bodei, L.; Kracmerova, T.; Luster, M.; Garin, E.; Herrmann, K. EANM Procedure Guideline for the Treatment of Liver Cancer and Liver Metastases with Intra-Arterial Radioactive Compounds. *Eur. J. Nucl. Med. Mol. Imaging* **2022**, *49*, 1682−1699.

(11) Goislard de Monsabert, C.; Touchefeu, Y.; Guiu, B.; Campillo-Gimenez, B.; Farges, O.; Tougeron, D.; Baumgaertner, I.; Ayav, A.; Beuzit, L.; Pracht, M.; Lièvre, A.; Le Sourd, S.; Boudjema, K.; Rolland, Y.; Garin, E.; Boucher, E.; Edeline, J. Selective Internal Radiation Combined with Chemotherapy Maintains the Quality of Life in Intrahepatic Cholangiocarcinomas. *Curr. Oncol.* **2021**, *28*, 4530−4541.

(12) Pérez-López, A.; Martín-Sabroso, C.; Gómez-Lázaro, L.; Torres-Suárez, A. I.; Aparicio-Blanco, J. Embolization Therapy with Microspheres for the Treatment of Liver Cancer: State-of-the-Art of Clinical Translation. *Acta Biomater.* **2022**, *149*, 1−15.

(13) d'Abadie, P.; Hesse, M.; Louppe, A.; Lhommel, R.; Walrand, S.; Jamar, F. Microspheres Used in Liver Radioembolization: From Conception to Clinical Effects. *Molecules* **2021**, *26*, 3966.

(14) Bouvry, C.; Palard, X.; Edeline, J.; Ardisson, V.; Loyer, P.; Garin, E.; Lepareur, N. Transarterial Radioembolization (TARE) Agents beyond Y-90-Microspheres. *Biomed. Res. Int.* **2018**, *2018*, 1435302.

(15) Manas, D.; Bell, J. K.; Mealing, S.; Davies, H.; Baker, H.; Holmes, H.; Hubner, R. A. The Cost-Effectiveness of TheraSphere in Patients with Hepatocellular Carcinoma Who are Eligible for Transarterial Embolization. *Eur. J. Surg. Oncol.* **2021**, *47*, 401−408.

(16) Filippi, L.; Schillaci, O.; Bagni, O. (90)Y-Radioembolization of Hepatocellular Carcinoma from a Theranostic Perspective: towards a Personalized Approach. *Eur. J. Nucl. Med. Mol. Imaging* **2018**, *45*, 2238−2239.

(17) Levillain, H.; Bagni, O.; Deroose, C. M.; Dieudonné, A.; Gnesin, S.; Grosser, O. S.; Kappadath, S. C.; Kennedy, A.; Kokabi, N.; Liu, D. M.; Madoff, D. C.; Mahvash, A.; Martinez de la Cuesta, A.; Ng, D. C. E.; Paprottka, P. M.; Pettinato, C.; Rodríguez-Fraile, M.; Salem, R.; Sangro, B.; Strigari, L.; Sze, D. Y.; de Wit van der Veen, B. J.; Flamen, P. International Recommendations for Personalised Selective Internal Radiation Therapy of Primary and Metastatic Liver Diseases with Yttrium-90 Resin Microspheres. *Eur. J. Nucl. Med. Mol. Imaging* **2021**, *48*, 1570−1584.

(18) Arnold, C. A.; Pezhouh, M. K.; Lam-Himlin, D.; Pittman, M. E.; VandenBussche, C.; Voltaggio, L. Y-90-TheraSpheres: The New Look of Yttrium-90. *Am. J. Surg. Pathol.* **2019**, *43*, 688−694.

(19) Reinders, M. T. M.; Smits, M. L. J.; van Roekel, C.; Braat, A. J. A. T. Holmium-166 Microsphere Radioembolization of Hepatic Malignancies. *Semin. Nucl. Med.* **2019**, *49*, 237−243.

(20) Li, R.; Li, D.; Jia, G.; Li, X.; Sun, G.; Zuo, C. Diagnostic Performance of Theranostic Radionuclides Used in Transarterial Radioembolization for Liver Cancer. *Front. Oncol.* **2021**, *10*, 551622.

(21) Cvjetinović, Đ.; Prijović, Ž.; Janković, D.; Radović, M.; Mirković, M.; Milanović, Z.; Mojović, M.; Škalamera, Đ.; Vranješ-Đurić, S. Bioevaluation of Glucose-Modified Liposomes as a Potential Drug Delivery System for Cancer Treatment Using 177-Lu Radiotracking. *J. Controlled Release* **2021**, *332*, 301−311.

(22) Aleksandar, V.; Drina, J.; Magdalena, R.; Zorana, M.; Marija, M.; Dragana, S.; Sanja, V. D. Optimization of the Radiolabelling Method for Improved in vitro and in vivo Stability of (90)Y-Albumin microspheres. *Appl. Radiat. Isot.* **2020**, *156*, No. 108984.

(23) Zhang, C.; Xiang, B. The Underlying Mechanisms and Strategies of DNA Damage and Repair in Radiation Sialadenitis. *Oral Dis.* **2021**, DOI: 10.1111/odi.14078.

(24) Wu, M.; Shi, K.; Huang, R.; Liu, C.; Yin, L.; Yong, W.; Sun, J.; Wang, G.; Zhong, Z.; Gao, M. Facile Preparation of 177Lu-Microspheres for Hepatocellular Carcinoma Radioisotope Therapy. *Chin. Chem. Lett.* **2022**, *33*, 3492−3496.

(25) Chan, H. W.; Lo, Y. H.; Chang, D. Y.; Li, J. J.; Chang, W. Y.; Chen, C. H.; Chang, C. H.; Chen, C. L.; Wang, H. E.; Liu, R. S.; Wu, C. Y. Radiometal-Labeled Chitosan Microspheres as Transarterial Radioembolization Agents against Hepatocellular Carcinoma. *Gels* **2022**, *8*, 180.

https://doi.org/10.1021/acsami.2c19829
ACS Appl. Mater. Interfaces XXXX, XXX, XXX−XXX

(26) Wu, X.; Ge, L.; Shen, G.; He, Y.; Xu, Z.; Li, D.; Mu, C.; Zhao, L.; Zhang, W. (131)I-Labeled Silk Fibroin Microspheres for Radioembolic Therapy of Rat Hepatocellular Carcinoma. *ACS Appl. Mater. Interfaces* **2022**, *14*, 21848−21859.
(27) Shi, X.; Li, Q.; Zhang, C.; Pei, H.; Wang, G.; Zhou, H.; Fan, L.; Yang, K.; Jiang, B.; Wang, F.; Zhu, R. Semiconducting Polymer Nano-Radiopharmaceutical for Combined Radio-Photothermal Therapy of Pancreatic Tumor. *J. Nanobiotechnol.* **2021**, *19*, 337.
(28) Datta, N. R.; Ordóñez, S. G.; Gaipl, U. S.; Paulides, M. M.; Crezee, H.; Gellermann, J.; Marder, D.; Puric, E.; Bodis, S. Local Hyperthermia Combined with Radiotherapy and/or Chemotherapy: Recent Advances and Promises for the Future. *Cancer Treat. Rev.* **2015**, *41*, 742−753.
(29) Zhang, Y.; Zhang, S.; Zhang, Z.; Ji, L.; Zhang, J.; Wang, Q.; Guo, T.; Ni, S.; Cai, R.; Mu, X.; Long, W.; Wang, H. Recent Progress on NIR-II Photothermal Therapy. *Front. Chem.* **2021**, *9*, No. 728066.
(30) Li, J.; Zhang, W.; Ji, W.; Wang, J.; Wang, N.; Wu, W.; Wu, Q.; Hou, X.; Hu, W.; Li, L. Near Infrared Photothermal Conversion Materials: Mechanism, Preparation, and Photothermal Cancer Therapy Applications. *J. Mater. Chem. B* **2021**, *9*, 7909−7926.
(31) Park, K. Y.; Han, H. S.; Hong, J. Y.; Seo, S. J.; Lee, S. J. Gold Nanoshell-Mediated Photothermal Therapy for Acne Vulgaris. *Dermatol. Ther.* **2020**, *33*, No. e13189.
(32) Doughty, A.; Hoover, A.; Layton, E.; Murray, C.; Howard, E.; Chen, W. Nanomaterial Applications in Photothermal Therapy for Cancer. *Materials* **2019**, *12*, 779.
(33) Tong, X.; Wang, Z.; Sun, X.; Song, J.; Jacobson, O.; Niu, G.; Kiesewetter, D. O.; Chen, X. Size Dependent Kinetics of Gold Nanorods in EPR Mediated Tumor Delivery. *Theranostics* **2016**, *6*, 2039−2051.
(34) Liu, Q.; Qian, Y.; Li, P.; Zhang, S.; Liu, J.; Sun, X.; Fulham, M.; Feng, D.; Huang, G.; Lu, W.; Song, S. I-131-Labeled Copper Sulfide-Loaded Microspheres to Treat Hepatic Tumors via Hepatic Artery Embolization. *Theranostics* **2018**, *8*, 785−799.
(35) Liu, Y.; Ai, K.; Lu, L. Polydopamine and its Derivative Materials: Synthesis and Promising Applications in Energy, Environmental, and Biomedical Fields. *Chem. Rev.* **2014**, *114*, 5057−5115.
(36) Liu, Y.; Ai, K.; Liu, J.; Deng, M.; He, Y.; Lu, L. Dopamine-Melanin Colloidal Nanospheres: an Efficient Near-Infrared Photothermal Therapeutic Agent for in vivo Cancer Therapy. *Adv. Mater.* **2013**, *25*, 1353−1359.
(37) Deng, Z.; Shang, B.; Peng, B. Polydopamine Based Colloidal Materials: Synthesis and Applications. *Chem. Rec.* **2018**, *18*, 410−432.
(38) Cheng, W.; Zeng, X.; Chen, H.; Li, Z.; Zeng, W.; Mei, L.; Zhao, Y. Versatile Polydopamine Platforms: Synthesis and Promising Applications for Surface Modification and Advanced Nanomedicine. *ACS Nano* **2019**, *13*, 8537−8565.
(39) Jin, A.; Wang, Y.; Lin, K.; Jiang, L. Nanoparticles Modified by Polydopamine: Working as ″Drug″ Carriers. *Bioact. Mater.* **2020**, *5*, 522−541.
(40) Zeng, X. W.; Luo, M. M.; Liu, G.; Wang, X. S.; Tao, W.; Lin, Y. X.; Ji, X. Y.; Nie, L.; Mei, L. Polydopamine-Modified Black Phosphorous Nanocapsule with Enhanced Stability and Photothermal Performance for Tumor Multimodal Treatments. *Adv. Sci.* **2018**, *5*, 1800510.
(41) Sun, G.; Wang, T.; Li, X.; Li, D.; Peng, Y.; Wang, X.; Jia, G.; Su, W.; Cheng, C.; Yang, J.; Zuo, C. Sub-Micrometer Au@PDA-I-125 Particles as Theranostic Embolism Beads for Radiosensitization and SPECT/CT Monitoring. *Adv. Healthcare Mater.* **2018**, *7*, 1800375.
(42) Huang, D.; Dai, H.; Tang, K.; Chen, B.; Zhu, H.; Chen, D.; Li, N.; Wang, Y.; Liu, C.; Huang, Y.; Yang, J.; Zhang, C.; Lin, R.; He, W. A Versatile UCST-Type Composite Microsphere for Image-Guided Chemoembolization and Photothermal Therapy Against Liver Cancer. *Nanoscale* **2020**, *12*, 20002−20015.
(43) Vivero-Escoto, J. L.; Slowing, I. I.; Trewyn, B. G.; Lin, V. S. Y. Mesoporous Silica Nanoparticles for Intracellular Controlled Drug Delivery. *Small* **2010**, *6*, 1952−1967.
(44) Lee, H.; Dellatore, S. M.; Miller, W. M.; Messersmith, P. B. Mussel-Inspired Surface Chemistry for Multifunctional Coatings. *Science* **2007**, *318*, 426−430.
(45) De La Vega, J. C.; Esquinas, P. L.; Rodríguez-Rodríguez, C.; Bokharaei, M.; Moskalev, I.; Liu, D.; Saatchi, K.; Häfeli, U. O. Radioembolization of Hepatocellular Carcinoma with Built-In Dosimetry: First in vivo Results with Uniformly-Sized, Biodegradable Microspheres Labeled with (188)Re. *Theranostics* **2019**, *9*, 868−883.
(46) Qian, Y.; Liu, Q.; Li, P.; Han, Y.; Zhang, J.; Xu, J.; Sun, J.; Wu, A.; Song, S.; Lu, W. Highly Tumor-Specific and Long-Acting Iodine-131 Microbeads for Enhanced Treatment of Hepatocellular Carcinoma with Low-Dose Radio-Chemoembolization. *ACS Nano* **2021**, *15*, 2933−2946.
(47) Giannini, E. G.; Testa, R.; Savarino, V. Liver Enzyme Alteration: a Guide for Clinicians. *Can. Med. Assoc. J.* **2005**, *172*, 367−379.

https://doi.org/10.1021/acsami.2c19829
ACS Appl. Mater. Interfaces XXXX, XXX, XXX−XXX